Received: 5 February 2020 | Revised: 26 May 2020 | Accepted: 30 May 2020

DOI: 10.1002/ardp.202000023

FULL PAPER

DPhG ARCH PHARM Archiv der Pharmazie

New 1,2,3-triazole–(thio)barbituric acid hybrids as urease inhibitors: Design, synthesis, in vitro urease inhibition, docking study, and molecular dynamic simulation

Mohammad S. Asgari[1] | Homa Azizian[2] | Mohammad Nazari Montazer[3] | Maryam Mohammadi-Khanaposhtani[4] | Mehdi Asadi[3] | Saghi Sepehri[5] | Parviz R. Ranjbar[1] | Rahmatollah Rahimi[6] | Mahmood Biglar[7] | Bagher Larijani[7] | Massoud Amanlou[3] | Mohammad Mahdavi[7]

[1]School of Chemistry, College of Science, University of Tehran, Tehran, Iran

[2]Department of Medicinal Chemistry, School of Pharmacy-International Campus, Iran University of Medical Sciences, Tehran, Iran

[3]Department of Medicinal Chemistry, Faculty of Pharmacy and Pharmaceutical Sciences Research Center, Tehran University of Medical Sciences, Tehran, Iran

[4]Cellular and Molecular Biology Research Center, Health Research Institute, Babol University of Medical Sciences, Babol, Iran

[5]Department of Medicinal Chemistry, School of Pharmacy, Ardabil University of Medical Sciences, Ardabil, Iran

[6]Department of Chemistry, Iran University of Science and Technology, Tehran, Iran

[7]Endocrinology and Metabolism Research Center, Endocrinology and Metabolism Clinical Sciences Institute, Tehran University of Medical Sciences, Tehran, Iran

Correspondence
Massoud Amanlou, Department of Medicinal Chemistry, Faculty of Pharmacy and Pharmaceutical Sciences Research Center, Tehran University of Medical Sciences, Tehran, Iran.
Email: Amanlou@tums.ac.ir

Mohammad Mahdavi, Endocrinology and Metabolism Research Center, Endocrinology and Metabolism Clinical Sciences Institute, Tehran University of Medical Sciences, Tehran 1417653761, Iran.
Email: momahdavi@tums.ac.ir

Abstract

A new series of 1,2,3-triazole–(thio)barbituric acid hybrids **8a**–**n** was designed and synthesized on the basis of potent pharmacophores with urease inhibitory activity. Therefore, these compounds were evaluated against *Helicobacter pylori* urease. The obtained result demonstrated that all the synthesized compounds, **8a**–**n**, were more potent than the standard urease inhibitor, hydroxyurea. Moreover, among them, compounds **8a**, **8c**–**e**, **8g**,**h**, and **8k**,**l** exhibited higher urease inhibitory activities than the other standard inhibitor used: thiourea. Docking studies were performed with the synthesized compounds. Furthermore, molecular dynamic simulation of the most potent compounds, **8e** and **8l**, showed that these compounds interacted with the conserved residues Cys592 and His593, which belong to the active site flap and are essential for enzymatic activity. These interactions have two consequences: (a) blocking the movement of a flap at the entrance of the active site channel and (b) stabilizing the closed active site flap conformation, which significantly reduces the catalytic activity of urease. Calculation of the physicochemical and topological properties of the synthesized compounds **8a**–**n** predicted that all these compounds can be orally active. The ADME prediction of compounds **8a**–**n** was also performed.

KEYWORDS

1,2,3-triazole, barbituric acid, docking study, molecular dynamic simulation, thiobarbituric acid, urease inhibition

1 | INTRODUCTION

Gastric disorders such as ulceration, gastritis, gastric carcinomas, and primary gastric lymphomas are etiologically related with *Helicobacter pylori* infections.[a] *H. pylori* is a Gram-negative microaerophilic bacterium that infects up to 50% of the world's human population.[2] The use of a triple therapy containing two antibiotic and a proton pump inhibitor is the most common treatment for *H. pylori* infection. However, drug resistance of *H.* pylori against antibiotics is rising sharply, and the design of new agents with various therapeutic mechanisms in this area is an attractive target for pharmacists.[3] Urease (EC 3.5.1.5) is the main enzyme for the hydrolysis of urea into ammonia, and given that this process is an essential pathway for the energy supply of bacteria, inhibition of urease can be useful for the elimination of bacteria. In this regard, several studies have demonstrated that urease inhibitors can be useful for treatment of *H. pylori* infection.[4]

Barbituric acid derivatives have various biological properties such as sedative–hypnotic, antimicrobial, antifungal, anticancer, anticonvulsant, and anti-urease properties.[5–10] However, another important scaffold in designing new bioactive compounds is the 1,2,3-triazole ring.[11] There are several reports in the literature concerning urease inhibitory activity of barbituric acid derivatives and 1,2,3-triazole derivatives.[12–17] For example, our research team has already reported 5-methylene (thio)barbituric acid derivative **A** and 1,2,3-triazole derivative **B** with a high inhibitory activity against *H. pylori* urease (Figure 1).[15,16] Therefore, in continuation of our efforts to derive new potent urease inhibitors, 1,2,3-triazole–(thio) barbituric acid hybrids **8a–n** were designed and synthesized via a click reaction. These compounds were evaluated against *H. pylori* urease. Furthermore, docking and molecular dynamic studies were performed to further investigate the interaction, orientation, and conformation of these compounds at the active site of urease.

2 | RESULTS AND DISCUSSION

2.1 | Chemistry

The synthetic route for the preparation of 1,2,3-triazole–(thio)-barbituric acid hybrids **8a–n** has been depicted in Scheme 1. Initially, a mixture of 4-hydroxy-3-methoxybenzaldehyde **1** and propargyl bromide **2** in the presence of K_2CO_3 in dimethylformamide was stirred for 3 hr at room temperature to afford 3-methoxy-4-(prop-2-ynyloxy)benzaldehyde **3**. In contrast, benzyl azides **5a–i** were produced in situ from reaction between benzyl bromides **4a–i** and NaN_3 in the presence of NEt_3. Then, 1,2,3-triazole derivatives **6a–i** were synthesized via a click reaction between benzyl azides **5a–i**, compound **3**, sodium ascorbate, and $CuSO_4{\cdot}5H_2O$ at room temperature for 16–24 h. Finally, compounds **6** reacted with barbituric acid **7a** or thiobarbituric acid **7b** in ethanol and piperidine to give the desired compounds **8a–n**.

2.2 | Urease inhibition

1,2,3-Triazole–(thio)barbituric acid hybrids **8a–n** were evaluated for their in vitro inhibitory activities against *H. pylori* urease in comparison with standard inhibitors hydroxyurea and thiourea (Table 1). The IC_{50} values of compounds **8a–n** (IC_{50} values = 8.10–76.53 μM)

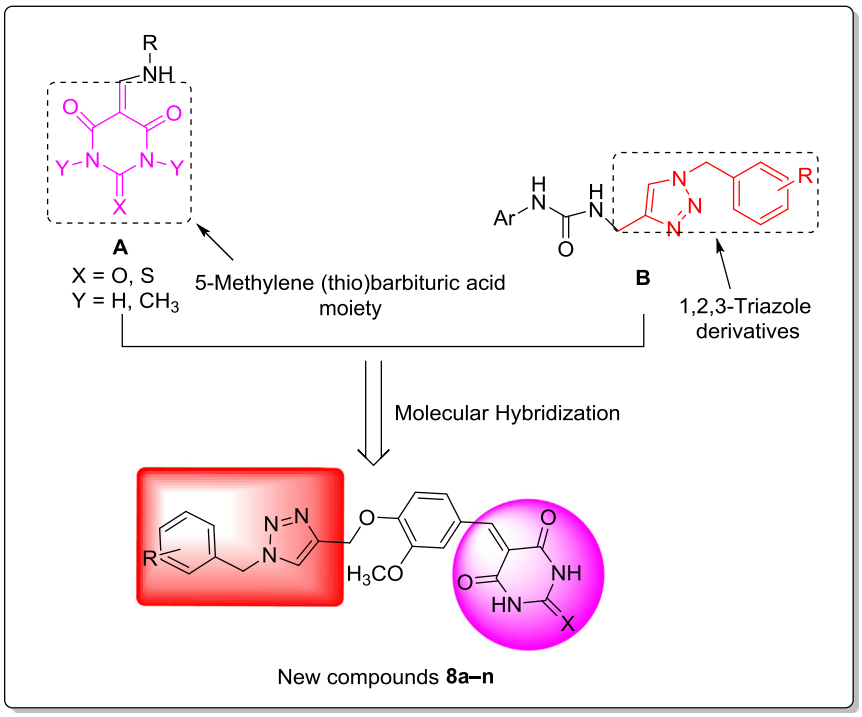

FIGURE 1 The design strategy for 1,2,3-triazole–(thio)barbituric acid hybrids **8a–n**

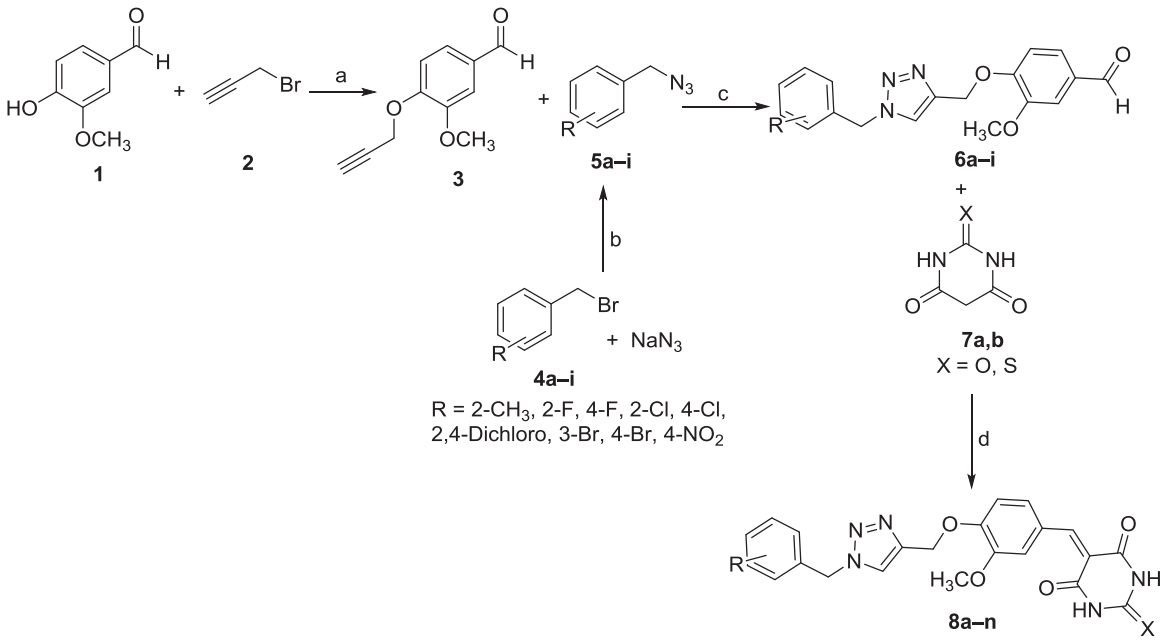

SCHEME 1 The synthesis procedure for compounds **8a**–**n**. Reagents and conditions: (a) K_2CO_3, dimethylformamide, room temperature, 3hr; (b) NaN_3, NEt_3, H_2O/*t*- (1:1), room temperature, 1hr; (c) sodium ascorbate, $CuSO_4{\cdot}5H_2O$, room temperature, 16–24hr; (d) ethanol, piperidine, room temperature, 24hr

demonstrated that they were all superior to that of hydroxyurea (IC_{50} value = 100 ± 0.2 μM). Also, 8 compounds **8a**, **8c**–**e**, **8g**,**h**, and **8k**,**l** of 14 synthesized compounds were more potent than thiourea against urease (IC_{50} value = 22.0 ± 0.03 μM). Among the synthesized compounds, the most potent compounds were compounds **8l** and **8e** with IC_{50} values = 8.102 and 8.30 μM, respectively.

Structurally, the title compounds are divided into two series: barbituric acid derivatives **8a**–**i** and thiobarbituric acid derivatives **8j**–**n**. In each series, the substituent on the pendant phenyl ring was altered to optimize the anti-urease activity. Among the barbituric acid derivatives, the most potent compound was compound **8e** with 4-chloro substituent on pendant phenyl ring. A change in the position of chlorine atom on the phenyl ring from C_4 to C_2, producing compound **8d** (IC_{50} value = 10.22 μM), slightly diminished the inhibitory activity, whereas the introduction of the second chloro substituent on C_2 of pendant phenyl ring of compound **8e**, as in 2,4-dichloro derivative **8f**, led to a significant decrease in the activity inhibitory activity. The second most potent compound in this series was

TABLE 1 The urease inhibitory activity of 1,2,3-triazole–(thio)barbituric acid hybrids **8a**–**n**

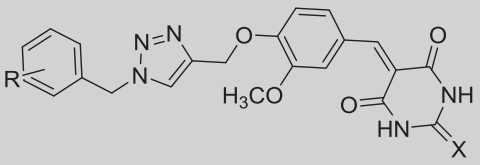

Compound	X	R	IC_{50} (μM)[a]	Compound	X	R	IC_{50} (μM)[a]
8a	O	2-CH_3	9.32 ± 0.16	**8i**	O	4-NO_2	24.38 ± 0.22
8b	O	2-F	45.03 ± 0.41	**8j**	S	2-CH_3	47.96 ± 0.53
8c	O	4-F	16.76 ± 0.25	**8k**	S	2-F	12.01 ± 0.21
8d	O	2-Cl	10.22 ± 0.13	**8l**	S	2-Cl	8.10 ± 0.17
8e	O	4-Cl	8.30 ± 0.09	**8m**	S	4-Cl	25.70 ± 0.32
8f	O	2,4-Dichloro	31.58 ± 0.32	**8n**	S	3-Br	76.53 ± 0.46
8g	O	3-Br	14.81 ± 0.15	Hydroxyurea	–	–	100 ± 0.20
8h	O	4-Br	13.63 ± 0.24	Thiourea	–	–	22.0 ± 0.03

[a]Values are the mean ± standard error of the mean. All experiments were performed at least three times.

2-methyl derivative **8a**. The replacement of 2-methyl substituent with 2-fluoro substituent dramatically decreased activity against urease, as observed in compound **8b**. The movement of fluoro substituent from 2-position to 4-position of pendant phenyl group caused a significant increase in the inhibitory activity. Bromosubstituted compounds **8g** and **8h** showed an approximately same inhibitory activity against urease. Inhibitory activities of these compounds were more than thiourea, and the inhibitory activity of 4-nitro derivative **8i** was slightly lower than thiourea.

Among the thiobarbituric acid derivatives **8j**–**n**, the most potent compound was 2-chloro derivative **8l**. This compound was also the most potent compound among the synthesized compounds **8a**–**n**. The replacement of chloro substituent with fluoro or methyl substituent, respectively, led to a slight decrease and a significant decrease in inhibition, whereas movement of chloro substituent from C_2 to C_4 of pendant phenyl ring, as in compound **8m**, led to a significant decrease in the inhibitory activity. Among the synthesized compounds, the less potent compound was 3-bromo derivative **8n** of thiobarbituric series.

The comparison of IC_{50} values of barbituric acid derivatives with their corresponding thiobarbituric acid analogs against *H. pylori* urease revealed that barbituric acid analogs **8a**, **8e**, and **8g**, respectively, with substituents 2-CH_3, 4-Cl, and 3-Br were more active than their thiobarbituric acid analogs **8j**, **8m**, and **8n**. In contrast, *H. pylori* urease inhibitory activity of 2-fluoro and 2-chloro derivatives **8b** and **8d** of barbituric acid series was less than their thiobarbituric acid analogs **8k** and **8l**.

2.3 | Kinetic study of urease inhibition

To determine urease inhibition type, a kinetic study was performed on the most potent compound **8l**. Moreover, urea was selected as a substrate. As can be seen in Figure 2a, Lineweaver–Burk plots demonstrated that compound **8l** inhibited urease in a competitive manner, as with increasing concentrations of this compound, V_{max} was not affected, but there was an increase in K_m. Furthermore, the value of the inhibition constant (K_i) for compound **8l** was calculated from secondary replotting of Lineweaver–Burk plots, and K_i was found to be 9.7 ± 0.02 μM (Figure 2b).

2.4 | Docking study

A docking study was carried out to understand the interaction modes of the synthesized compounds in the urease active site, and these interactions were compared with standard drug interaction in the active site. For this purpose, a crystal structure of urease from jack bean (JBU) with PDB ID: 4H9M was retrieved from RCSB Protein Data Bank (http://www.rcsb.org/pdb/home/home.do).[18,19] Acetohydroxamic acid (AHA) as a urease inhibitor is bound to the active site of JBU. Therefore, the reliability of the applied docking protocol was assessed by redocking of AHA into the active site of JBU. The key characteristic of a good docking program is its ability to reproduce the experimental or crystallographic binding modes of ligands. To test this, a ligand is taken out of the X-ray structure of its protein–ligand complex and redocked into its binding site. The docked binding mode is then compared with the experimental binding mode, and the root mean square deviation (RMSD) is calculated; a prediction of a binding mode is considered successful if the RMSD is below a certain value (usually <2.0 Å). The superimposed structures between the docked and the crystallographic AHA over JBU with an acceptable RMSD value within the cut-off limit (1.02 Å) are shown in Figure 3. This protocol was then similarly applied to all synthesized compounds, **8a**–**n**.

The performed docking procedure was then applied to evaluate the interaction between newly synthetized compounds, **8a**–**n**, at the JBU active site in comparison to thiourea as a reference urease inhibitor. The top scoring pose of all compounds

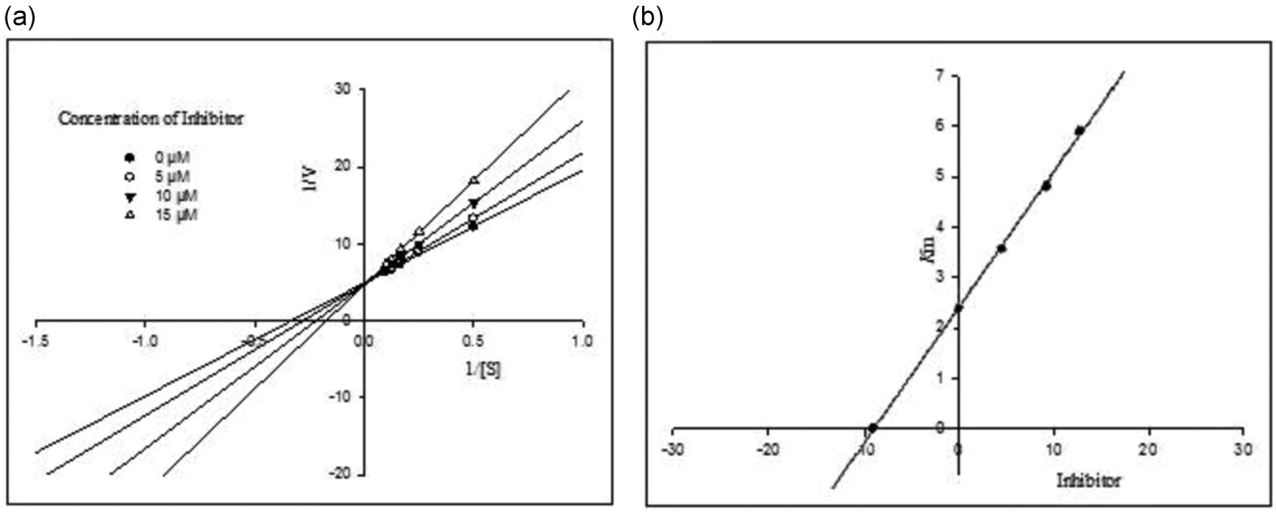

FIGURE 2 (a) Lineweaver–Burk plots for the inhibition of urease by compound **8l**; (b) secondary replotting of Lineweaver–Burk plots for determination of K_i

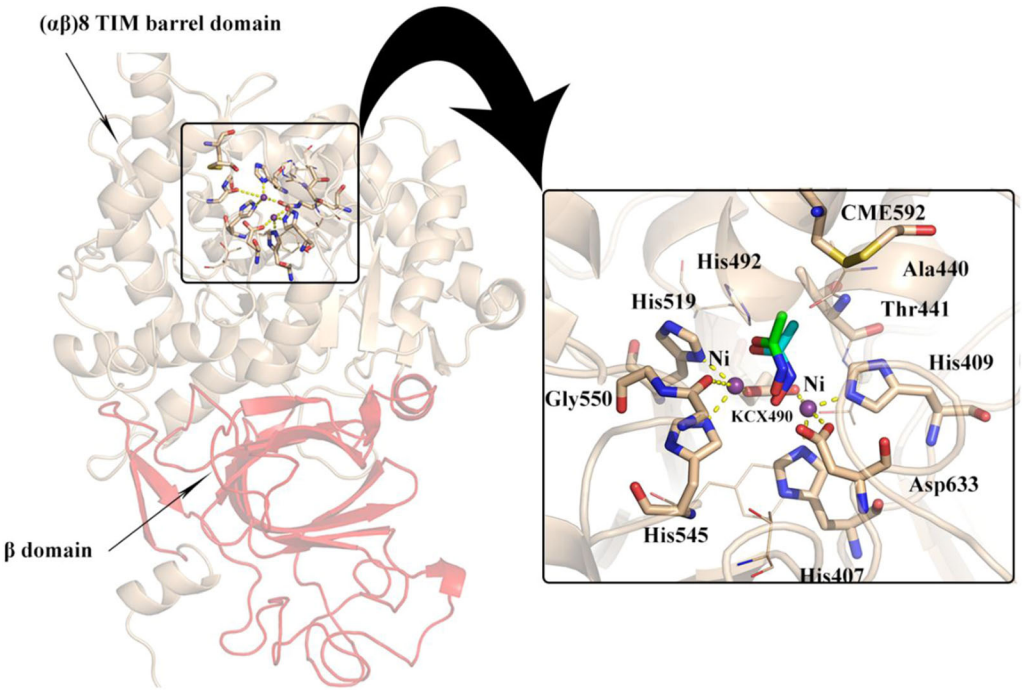

FIGURE 3 The location of jack bean urease active site over C-terminal $(\alpha\beta)_8$ TIM barrel domain. The inset shows a close-up representation of the active site; the acetohydroxamic acid co-crystallized and the corresponding redocked form are represented in green and cyan color, respectively

was analyzed inside the binding site of JBU. In the binding model, all the compounds are successfully occupied in the bi-nickel active site cavity.

Figure 4 shows that the fitting-in mechanism of barbituric acid and thio-barbiturate moiety in the active site of the enzyme is quite similar. The 1,2,3-triazol–benzylidene moiety adapts by a flexible conformation in the large hydrophobic opening of the active site pocket (Figure 4a), whereas the (thio)barbituric acid ring tends to orient toward the two nickel atoms through the ionized Ni (Ni^{2+}) and the carbonyl group at C_4 position of the (thio)barbiturate ring (Figure 4b), which is similar to the behavior of the carbonyl oxygens in the AHA.

Additionally, Figure 4b demonstrates that the thiobarbituric acid ring appears to make some distance deviation from the Ni–Ni center, which is due to the steric character of the sulfur atom.

2.5 | Molecular dynamic simulation

To understand the criteria for rational designing of urease inhibitors, it is necessary to uncover the structural perturbations incurred by the most potent compounds (compounds **8e** and **8l**) over urease and the effect of these compounds on the active site environment in comparison to thiourea as a urease inhibitor standard.

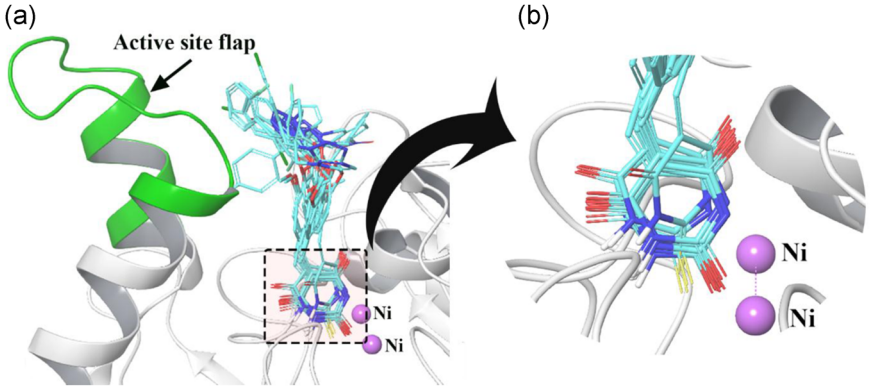

FIGURE 4 (a) A representation of the docking poses of compounds relative to bi-nickel center and active site flap over jack bean urease active site. (b) A close-up illustration of the (thio)barbiturate ring. The active site flap is shown in green color

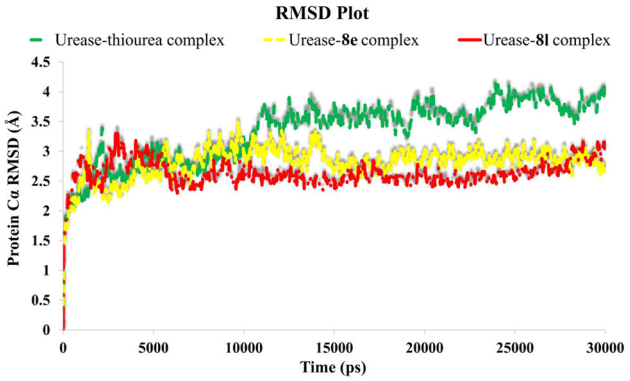

FIGURE 5 Root mean square deviation (RMSD) of the urease Cα complexed with thiourea (in green) and compounds **8e** (in yellow) and **8l** (in red) for over 30-ns MD simulation time

RMSD of the protein's backbone from its initial to final conformation is applied over 30 ns molecular dynamic (MD) simulation to study the stability of the protein–ligand complex. The RMSD value of each urease–ligand complex indicates that the employed simulation time has been enough to obtain an equilibrium structure over the simulation time (Figure 5). Thus, the structures at the MD equilibrium state are used to investigate the structural specificity of the ligand–protein complexes. The RMSD simulation showed that urease complexed with thiourea maintained an overall stability after 10 ns of MD simulation time with higher fluctuation stabilizing at an average of 3.75 Å (Figure 5, green line), whereas the bound state of compounds **8e** and **8l** displayed a longer equilibration time (after 7 ns of MD simulation) with obviously lower fluctuations (3 and 2.6 Å for the complex of **8e**–urease and **8l**–urease, respectively; Figure 5, yellow and red lines).

Root mean square fluctuation (RMSF) refers to the fluctuation of the Cα atom coordinates from its average position throughout the simulation. This indicates the flexibility of the protein backbone structure. Loops with loosely organized structure have high RMSF value while helixes and sheets represent lower RMSF value. Comparing RMSF values of urease–compound complexes shows that the residues of the flap region covering the active site, 590–606, would have significantly lower RMSF value in urease–**8e** and urease–**8l** rather than urease–thiourea complex (Figure 6a). Based on crystal structures of the ureases, besides the conserved residues in the active site, most of ureases share conserved residues that make up the mobile flap, which covers the active site.[20] In JBU, the residues comprising the mobile flap are 590–606 on α subunit part of the enzyme.

The other regions that have lower RMSF values in urease–**8e** and urease–**8l** complex were residues 435–440, 474, and 636–637 (Figure 6b).

Furthermore, Figure 6b shows that compounds **8e** and **8l** well occupied the active pockets of urease and tightly anchored the

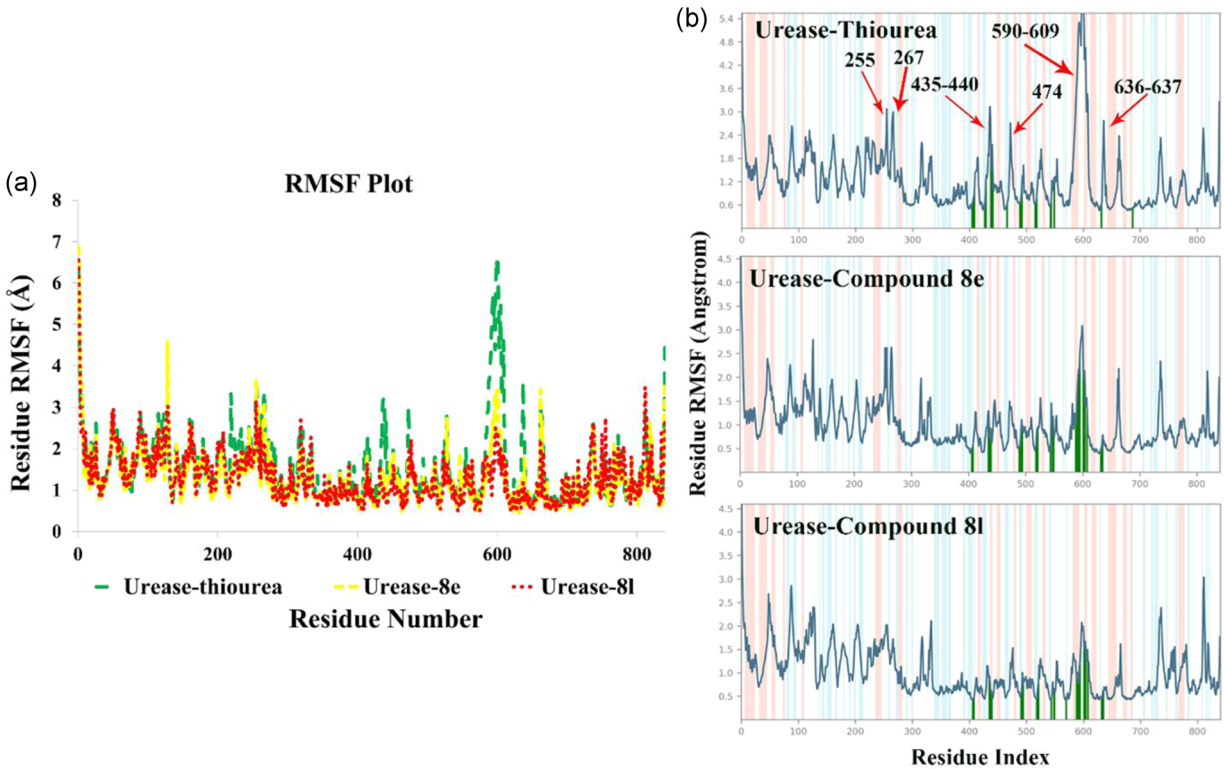

FIGURE 6 (a) RMSF of the urease Cα complexed with thiourea (in green), compounds **8e** (in yellow) and **8l** (in red); (b) ligand binding location for over 30 ns MD simulation time. The α-helical and β-strand regions are highlighted in red and blue backgrounds, respectively

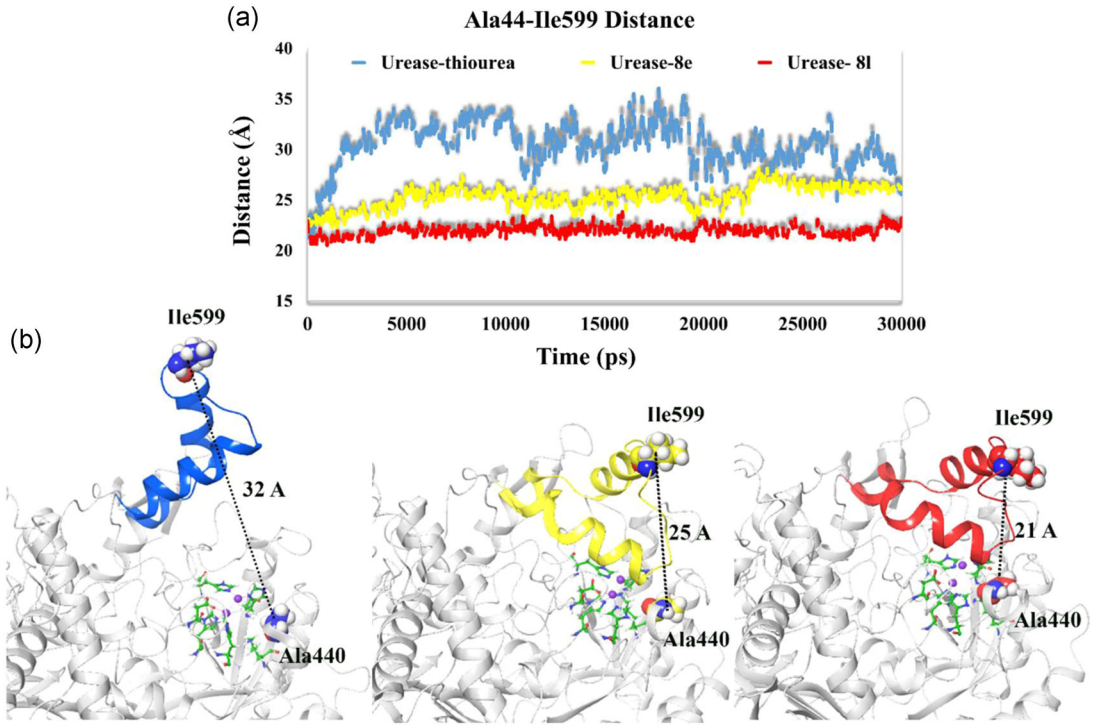

FIGURE 7 (a) MD simulated flap distance between Ala440 and Ile599 in thiourea (blue), compound **8e** (yellow), and compound **8l** (red) in urease-bound state. (b) Representative snapshots from MD simulations where the flap covering the active site can adopt open conformations of the flap (blue) and closed conformation (yellow and red). The zoomed image of the active site residues shows catalytic residues in green and nickel atoms in purple

helix-turn-helix motif over the active site cavity (vertical green line), which reduces the flexibility of flap residues (590–609) by interacting with key amino acid residues and results in the inhibition of urease activity.

To study the behavior of the active site covering flap over the course of the MD simulation, the distances between Ile599 at the tip of the flap and Ala440 at the entrance of the active site channel in the urease–compound complexes are recorded and analyzed. Figure 7a displays representative Ile599–Ala440 separations for the urease–compound complex. In the thiourea-bound state, the separation distance of these residues is about 32 Å, corresponding as open flap conformation, whereas in the case of compounds **8e** and **8l**, this distance varies only slightly, oscillating within 25 and 21 Å, respectively, which is related to the closed flap conformation (Figure 7b). Based on this closed flap conformation, it is proposed that compounds **8e** and **8l** inhibit urease activity by stabilizing the reaction intermediate during the ureolytic reaction.[21]

The molecular interactions of thiourea and the compounds **8e** and **8l** over the binding site of JBU are represented in Figure 8.

Thiourea was found to be deeply bound in the active site due to its smaller size, and it interacted with an ionic coordinated complex (two Ni ions complexed with all of their coordinated residues including His407, His409, His519, and His545; Figure 8a) for the first quarter part of MD simulation time, and for the rest of the simulation time, it formed an H-bond with Thr442, Thr467, and Cys405 through both of its NH_2 groups (Figure 8b).

Figure 8c shows barbituric acid ring of compound **8e** tightly coordinated along the metal bi-nickel center for the whole simulation time. For the first 20 ns of MD simulation time, the 5-benzylidine moiety and C_4 carbonyl group of barbituric acid ring formed a π–π stack and an H-bond with His593 and Cys592, respectively. Figure 8d shows that the mentioned contacts disappeared and were substituted by interactions with Phe605 and Arg609 from one part alongside with Arg349 and Ala440 at the other part of the active site cavity for the rest of the MD simulation time.

Compound **8l** depicts a similar orientation and interaction with **8e** (metal coordination forming through thiobarbituric acid ring, H-bond, and π–π stacking with Cys592 and His593, respectively), except that the two former interactions persisted for higher MD simulation time (48% and 56%, respectively; Figure 8e,f).

It is noteworthy that Cys592 is one of the key residues in the active site. Ligand interacting with Cys592 and His593 seems to be most important for urease inhibition due to a decrease in the flexibility of mobile flap covering the active site entrance, followed by inhibition of the ureolytic activity.

2.6 | Screening of pharmacokinetic properties

To predict the pharmacokinetic properties of target compounds **8a**–**n**, some of physicochemical properties of these compounds are calculated and listed in Table 2. Physicochemical properties

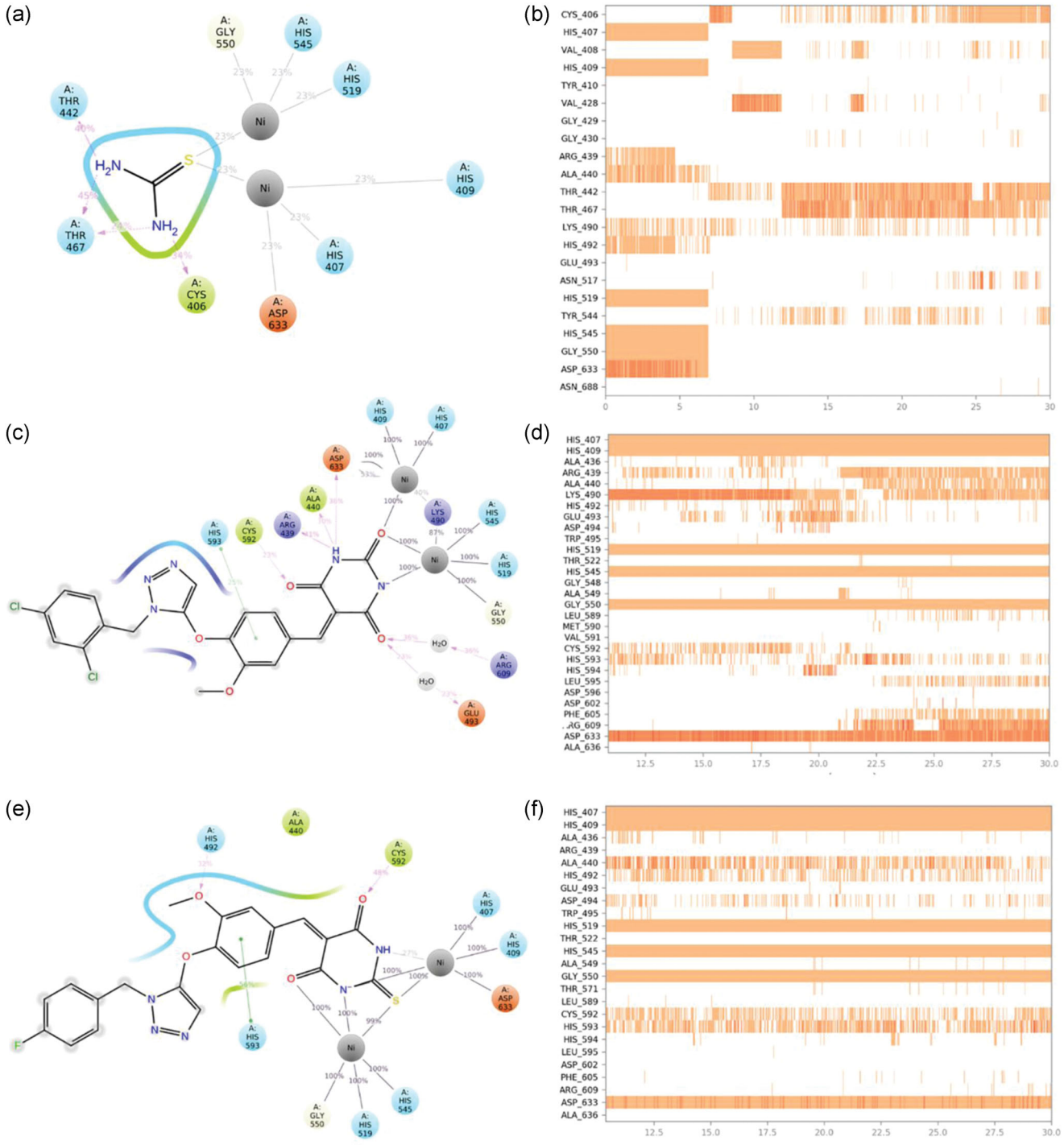

FIGURE 8 A two-dimensional (left columns) and timeline (right columns) representation of ligand–residue interactions that occur during the simulation time, which include urease-bound state of (a,b) thiourea, (c,d) compound **8e**, and (e,f) compound **8l**

included molecular weight, the number of H-bond acceptors (HBA), the number of H-bond donors (HBD), and octanol/water partition coefficients (log*P*). Moreover, the numbers of rotatable bonds (RBC) as a topological factor were collected (Table 2). One of the rules used to predict whether a drug is orally active is Lipinski's rule of 5 (MW ≤ 500, HBA ≤ 10, HBD ≤ 5, and log*P* ≤ 5).[22] A drug candidate should not violate more than one of Lipinski's rules to be active orally. As can be seen in Table 2, all the synthesized compounds passed Lipinski's rule. The RBC is a very good descriptor for oral bioavailability of drug candidates, and previous data revealed that compounds with RBC < 10 have a high oral bioavailability in rats.[23] As can be seen in Table 2, all the title compounds **8a**–**n** have RBC = 7, so it is expected that these compounds will have a good oral bioavailability.

TABLE 2 Physicochemical properties of the synthesized compounds **8a–n**

Compound	MW	HBA	HBD	Log*P*	RBC
8a	447.45	7	2	2.27	7
8b	451.41	7	2	1.95	7
8c	451.41	7	2	1.95	7
8d	467.87	7	2	2.35	7
8e	467.87	7	2	2.35	7
8f	502.31	7	2	2.9	7
8g	512.32	7	2	2.62	7
8h	512.32	7	2	2.62	7
8i	478.42	9	2	1.82	7
8j	463.51	6	2	2.82	7
8k	467.48	6	2	2.49	7
8l	483.93	6	2	2.89	7
8m	483.93	6	2	2.89	7
8n	528.38	6	2	3.16	7

Abbreviations: HBA, number of H-bond acceptors; HBD, number of H-bond donors; log*P*, the octanol–water partition coefficient; MW, molecular weight; RBC, number of rotatable bonds.

Absorption, distribution, metabolism, excretion, and toxicity (ADMET) prediction of the synthesized compounds **8a–n** was performed using online software PreADMET, and the obtained results are presented in Table 3. As can be seen in this table, compounds **8a–n** have poor permeability to Caco-2 cells and skin. Moreover, these compounds have high human oral absorption and protein-binding plasma. An in silico ADME study also predicted that these compounds did not have an inhibition effect on CYP3A4, CYP2C19, and CYP2D6; however, they probably inhibited CYP2C9. Furthermore, compounds **8a–n** can be substrates for CYP3A4. In contrast, these compounds are not a substrate for CYP2D6.

TABLE 4 Toxicity prediction of the synthesized compounds **8a–n**

Entry	Ames test	Carcino mouse	Carcino rat	hERG inhibition
8a	Mutagen	Negative	Positive	Medium risk
8b	Mutagen	Positive	Positive	Medium risk
8c	Mutagen	Positive	Positive	Medium risk
8d	Mutagen	Negative	Negative	Medium risk
8e	Mutagen	Negative	Negative	Medium risk
8f	Mutagen	Negative	Negative	Medium risk
8g	Mutagen	Negative	Positive	Medium risk
8h	Mutagen	Negative	Positive	Medium risk
8i	Mutagen	Negative	Positive	Medium risk
8j	Mutagen	Negative	Negative	Medium risk
8k	Mutagen	Negative	Positive	Medium risk
8l	Mutagen	Negative	Negative	Medium risk
8m	Mutagen	Negative	Negative	Medium risk
8n	Mutagen	Negative	Positive	Medium risk

TABLE 3 ADME prediction of the synthesized compounds **8a–n**

Entry	Caco-2[a]	HIA%[a]	Skin permeability[a]	PBP%[a]	CYP3A4 substrate	CYP3A4 inhibition	CYP2C9 inhibition	CYP2C19 inhibition	CYP2D6 substrate	CYP2D6 inhibition
8a	20.665	94.9864	−3.94844	87.9195	Substrate	Non	Inhibitor	Non	Non	Non
8b	20.907	94.3737	−4.21172	89.6537	Substrate	Non	Inhibitor	Non	Non	Non
8c	20.014	94.3737	−4.24112	87.4573	Substrate	Non	Inhibitor	Non	Non	Non
8d	20.883	96.7318	−4.004	88.7605	Substrate	Non	Inhibitor	Non	Non	Non
8e	20.305	96.7318	−4.03017	88.0221	Substrate	Non	Inhibitor	Non	Non	Non
8f	20.586	97.4518	−3.97189	88.4792	Substrate	Non	Inhibitor	Non	Non	Non
8g	20.648	97.3802	−3.89729	87.4305	Substrate	Non	Inhibitor	Non	Non	Non
8h	20.593	97.3802	−3.89845	87.4278	Substrate	Non	Inhibitor	Non	Non	Non
8i	17.469	71.9521	−3.78887	89.8316	Substrate	Non	Inhibitor	Non	Non	Non
8j	21.045	97.7060	−3.94447	97.7060	Substrate	Non	Inhibitor	Non	Non	Non
8k	21.014	97.5517	−4.20359	87.2295	Substrate	Non	Inhibitor	Non	Non	Non
8l	21.505	97.8670	−3.99523	88.8011	Substrate	Non	Inhibitor	Non	Non	Non
8m	20.987	97.8673	−4.02237	88.8991	Substrate	Non	Inhibitor	Non	Non	Non
8n	21.539	97.5362	−3.88953	89.9210	Substrate	Non	Inhibitor	Non	Non	Non

Abbreviations: ADME, absorption, distribution, metabolism, excretion; PBP, protein-binding plasma; HIA, human oral absorption.
[a]The recommended ranges for Caco-2: <25 is poor and >500 is great; HIA: >80% is high and <25% is poor; skin permeability: −8.0 to −1.0; and PBP: >80% is high and <25% is poor.

In terms of toxicity, PreADMET software predicted that all the synthesized compounds are mutagens and have medium risk for cardiotoxicity (hERG inhibition; Table 4). As can be seen in Table 4, compounds **8d**–**f**, **8j**, and **8l**,**m** do not have carcinogenic effects on mouse and rat, whereas compounds **8b**,**c** have carcinogenic effects on both of them. Furthermore, compounds **8a**, **8g**–**i**, **8k**, and **8n** do not have carcinogenic effects on mouse.

2.7 | Cytotoxicity

Cytotoxicity of the most active compounds, **8a**, **8e**, and **8l**, was evaluated against the human normal cell line HDF using 3-(4,5-dimethylthiazol-2-yl)-2,5-diphenyl tetrazolium bromide (MTT) assay. This study revealed that at 200 μM, test compounds were non-cytotoxic against the HDF cell line.

3 | CONCLUSION

In general, the 1,2,3-triazole ring and (thio)barbituric acid as effective urease inhibitor pharmacophores were attached together. Fourteen derivatives of the 1,2,3-triazole–(thio)barbituric scaffold were synthesized and their inhibitory activity against *H. pylori* urease was determined. The obtained results demonstrated that all the synthesized compounds were more potent than standard inhibitor hydroxyurea and among them compounds **8a**, **8c**–**e**, **8g**,**h**, and **8k**,**l** were also more potent than standard inhibitor thiourea. Docking study of compounds **8a**–**n** showed that all these compounds successfully occupied the active site cavity of urease. Molecular dynamic simulation of the most potent compounds **8e** and **8l** proposed that these compounds inhibited urease activity by stabilizing the reaction intermediate during the ureolytic reaction. Furthermore, the title compounds **8a**–**n** can be orally active.

4 | EXPERIMENTAL

4.1 | Chemistry

4.1.1 | General

Melting points were taken on a Kofler hot-stage apparatus. ^{1}H and ^{13}C nuclear magnetic resonance (NMR) spectra (provided as Supporting Information Data) were recorded on Bruker FT-500, using tetramethylsilane as an internal standard. The infrared (IR) spectra were obtained on a Nicolet Magna FT-IR 550 spectrophotometer (KBr disks). Elemental analyses were carried out with an Elementar Analysensysteme GmbH VarioEL CHN mode. Compounds **3** and **5a**–**i** were obtained according to described pathway in our newly published article.[24,25]

The InChI keys of the investigated compounds, together with some biological activity data, are provided as Supporting Information Data.

4.1.2 | General procedure for the synthesis of 1,2,3-triazole derivatives (6a–i)

A mixture of 3-methoxy-4-(prop-2-ynyloxy)benzaldehyde **3** (1 mmol), sodium ascorbate, and $CuSO_4{\cdot}5H_2O$ (7 mol%) was added to the freshly prepared benzyl azide derivatives **5a**–**i**, and the obtained mixture was stirred at room temperature for 16–24 hr. Then, the reaction mixture was poured into crushed ice and precipitated products **6a**–**i** were filtered off, washed with cold water, and purified by recrystallization (ethyl acetate).

4.1.3 | General procedure for the synthesis of 1,2,3-triazole–(thio)barbituric acid hybrids 8a–n

The mixture of 1,2,3-triazole derivatives **6a**–**i** (0.5 mmol), (thio)barbituric acid derivatives **7a**,**b** (0.5 mmol), ethanol (2 ml), and piperidine (2 drops) was stirred at room temperature for 24 hr. Then, the reaction mixture was poured into cold ware and obtained precipitates were dried after filtration to obtain pure products **8a**–**n**.

*5-(3-Methoxy-4-{[1-(2-methylbenzyl)-1H-1,2,3-triazol-5-yl]methoxy}-benzylidene)pyrimidine-2,4,6(1H,3H,5H)-trione (**8a**)*

White solid; yield: 66%, mp: 185–190°C. IR (KBr): 1,702 (C═O), 1,627 (C═C alkene), 2,940 (C–H aromatic) cm^{-1}. ^{1}H NMR (500 MHz, dimethyl sulfoxide [DMSO]-d_6) δ 2.21 (s, 3H, CH_3), 3.60 (s, 3H, OCH_3), 5.03 (S, 2H, N–CH_2), 5.67 (s, 2H, O–CH_2), 5.91 (s, 1H, alkene), 6.55 (d, J = 6.3 Hz, 1H, Ar), 6.63 (s, 1H, Ar), 6.87 (d, J = 7.5 Hz, 1H, Ar), 7.07 (d, J = 6.4 Hz, 1H, Ar), 7.32–7.12 (m, 3H, Ar), 8.13 (s, 1H, triazole), 9.99 (s, 2H, NH) ppm. ^{13}C NMR (126 MHz, DMSO) δ 18.09, 50.39, 54.8, 61.4, 111.1, 113.1, 115.0, 115.1, 122.4, 122.7, 124.4, 130.2, 137.8, 142.8, 144.3, 147.9, 150.2, 158.5, 160.5, 163.7, 165.3 ppm. Anal. calcd. for $C_{23}H_{21}N_5O_5$: C, 61.74; H, 4.73; N, 15.65. Found: C, 61.58; H, 4.83; N, 15.49.

*5-(4-{[1-(2-Fluorobenzyl)-1H-1,2,3-triazol-5-yl]methoxy}-3-methoxybenzylidene)pyrimidine-2,4,6(1H,3H,5H)-trione (**8b**)*

White solid; yield: 59%; mp: 208–213°C. IR (KBr): 1,705 (C═O), 1,636 (C═C alkene), 2,924 (C–H aromatic) cm^{-1}. ^{1}H NMR (500 MHz, DMSO-d_6) δ 3.60 (s, 3H, OCH_3), 5.03 (s, 2H, N–CH_2), 5.67 (s, 2H, O–CH_2), 5.92 (s, 1H, alkene), 6.56 (d, J = 8.1 Hz, 1H, Ar), 6.64 (s, 1H, Ar), 6.89 (d, J = 8.2 Hz, 1H, Ar), 7.24 (dt, J = 15.3, 8.4 Hz, 2H, Ar), 7.33 (t, J = 7.3 Hz, 1H, Ar), 7.45–7.38 (m, 1H, Ar), 8.23 (s, 1H, triazole), 10.08 (s, 2H, NH) ppm. ^{13}C NMR (126 MHz, DMSO) δ 46.3, 54.8, 61.4, 111.1, 113.1, 115.0, 115.1, 122.4, 122.7, 124.4, 130.2, 137.8, 142.8, 144.3, 147.9, 150.2, 158.5, 160.5, 163.7, 165.3 ppm. Anal. calcd. for $C_{22}H_{18}FN_5O_5$: C, 58.54; H, 4.02; N, 15.51. Found: C, 58.41; H, 4.16; N, 15.39.

*5-(4-{[1-(4-Fluorobenzyl)-1H-1,2,3-triazol-5-yl]methoxy}-3-methoxybenzylidene)pyrimidine-2,4,6(1H,3H,5H)-trione (**8c**)*

White solid; yield: 79%, mp: 116–118°C. IR (KBr): 1,716 (C═O), 1,649 (C═C alkene), 2,921 (C–H aromatic) cm^{-1}. ^{1}H NMR (500 MHz,

DMSO-d_6) δ 3.59 (s, 3H, OCH_3), 5.01 (s, 2H, N–CH_2), 5.81 (s, 2H, O–CH_2), 5.92 (s, 1H, alkene), 6.53 (d, J = 8.3 Hz, 1H, Ar), 6.59 (s, 1H, Ar), 6.89 (d, J = 8.4 Hz, 1H, Ar), 7.06 (s, 1H, Ar), 7.39 (d, J = 8.7 Hz, 1H, Ar), 7.48 (t, J = 8.0 Hz, 2H, Ar), 8.18 (s, 1H, triazole), 9.86 (s, 2H, NH). ^{13}C NMR (126 MHz, DMSO) δ 44.07, 48.02, 54.95, 112.16, 113.17, 118.30, 120.30, 120.32, 124.28, 124.86, 125.22, 128.42, 129.83, 131.07, 131.15, 135.39, 136.38, 142.26, 144.55, 148.00, 172.27, 173.62 ppm. Anal. calcd. for $C_{22}H_{18}FN_5O_5$: C, 58.54; H, 4.02; N, 15.51. Found: C, 58.39; H, 4.15; N, 15.68.

*5-(4-{[1-(2-Chlorobenzyl)-1*H*-1,2,3-triazol-5-yl]methoxy}-3-methoxybenzylidene)pyrimidine-2,4,6(1*H*,3*H*,5*H*)-trione (**8d**)*

White solid; yield: 76%, mp: 196–200°C. IR (KBr): 1,680 (C═O), 1,645 (C═C alkene), 2,926 (C–H aromatic) cm^{-1}. ^{1}H NMR (500 MHz, DMSO-d_6) δ 3.60 (s, 3H, OCH_3), 5.05 (s, 2H, N–CH_2), 5.72 (s, 2H, O–CH_2), 5.92 (s, 1H, alkene), 6.57 (d, J = 8.3 Hz, 1H, Ar), 6.64 (s, 1H, Ar), 6.89 (d, J = 8.4 Hz, 1H, Ar), 7.19 (d, J = 8.6 Hz, 1H, Ar), 7.38 (dt, J = 19.7, 7.1 Hz, 2H, Ar), 7.52 (d, J = 7.7 Hz, 1H, Ar), 8.22 (s, 1H, triazole), 10.06 (s, 2H, NH). ^{13}C NMR (126 MHz, DMSO) δ 43.3, 50.0, 54.9, 61.4, 90.5, 111.0, 111.1, 113.1, 113.2, 118.3, 124.5, 127.2, 129.0, 132.0, 133.0, 137.8, 142.9, 144.5, 147.9, 150.2, 163.2, 163.7, 165.3 ppm. Anal. calcd. for $C_{22}H_{18}ClN_5O_5$: C, 56.48; H, 3.88; N, 14.97. Found: C, 56.57; H, 3.74; N, 14.86.

*5-(4-{[1-(4-Chlorobenzyl)-1*H*-1,2,3-triazol-5-yl]methoxy}-3-methoxybenzylidene)pyrimidine-2,4,6(1*H*,3*H*,5*H*)-trione (**8e**)*

White solid; yield: 70%, mp: 189–194°C. IR (KBr): 1,705 (C═O), 1,597 (C═C alkene), 2,966 (C–H aromatic) cm^{-1}. ^{1}H NMR (500 MHz, DMSO-d_6) δ 3.60 (s, 3H, OCH_3), 5.04 (s, 2H, N–CH_2), 5.70 (s, 2H, O–CH_2), 5.91 (s, 1H, alkene), 6.88 (s, 1H, Ar), 7.29 (s, 2H, Ar), 7.47 (s, 2H, Ar), 7.69 (s, 1H, Ar), 8.24 (s, 1H, triazole), 9.86 (s, 1H, NH), 10.06 (s, 1H, NH). ^{13}C NMR (126 MHz, DMSO) δ 49.5, 54.9, 60.9, 109.2, 111.1, 112.2, 113.2, 118.3, 124.5, 125.8, 127.3, 128.5, 130.9, 133.0, 137.6, 142.5, 144.9, 147.4, 150.3, 162.1, 165.3 ppm. Anal. calcd. for $C_{22}H_{18}ClN_5O_5$: C, 56.48; H, 3.88; N, 14.97. Found: C, 56.31; H, 3.71; N, 15.08.

*5-(4-{[1-(2,4-Dichlorobenzyl)-1*H*-1,2,3-triazol-5-yl]methoxy}-3-methoxybenzylidene)pyrimidine-2,4,6(1*H*,3*H*,5*H*)-trione (**8f**)*

White solid; yield: 74%, mp: 200–203°C. IR (KBr): 1,700 (C═O), 1,626 (C═C alkene), 2,926 (C–H aromatic) cm^{-1}. ^{1}H NMR (500 MHz, DMSO-d_6) δ 3.81 (s, 3H, OCH_3), 5.27 (s, 2H, N–CH_2), 5.73 (s, 2H, O–CH_2), 5.99 (s, 1H, alkene), 7.32 (s, 1H, Ar), 7.40 (s, 2H, Ar), 7.48 (s, 1H, Ar), 7.56 (s, 1H, Ar), 7.72 (s, 1H, Ar), 8.32 (s, 1H, triazole), 9.65–10.00 (m, 2H, NH). ^{13}C NMR (126 MHz, DMSO) δ 49.6, 54.9, 61.1, 109.7, 112.2, 125.0, 125.2, 127.4, 128.6, 129.4, 131.5, 133.5, 141.6, 146.2, 152.2, 166.8, 168.7 ppm. Anal. calcd. for $C_{22}H_{17}Cl_2N_5O_5$: C, 52.61; H, 3.41; N, 13.94. Found: C, 52.75; H, 3.62; N, 14.05.

*5-(4-{[1-(3-Bromobenzyl)-1*H*-1,2,3-triazol-5-yl]methoxy}-3-methoxybenzylidene)pyrimidine-2,4,6(1*H*,3*H*,5*H*)-trione (**8g**)*

White solid; yield: 75%, mp: 212–214°C. IR (KBr): 1,692 (C═O), 1,646 (C═C alkene), 1,156, 2,925 (C–H aromatic) cm^{-1}. ^{1}H NMR (500 MHz, DMSO-d_6) δ 3.60 (s, 3H, OCH_3), 5.04 (s, 2H, N–CH_2), 5.62 (s, 2H, O–CH_2), 5.92 (s, 1H, alkene), 6.56 (s, 1H, Ar), 6.64 (s, 1H, Ar), 6.87 (s, 1H, Ar), 7.30 (s, 1H, Ar), 7.32 (d, J = 7.7 Hz, 1H, Ar), 7.55 (s, 2H, Ar), 8.28 (s, 1H, triazole), 10.13 (s, 2H, NH). ^{13}C NMR (126 MHz, DMSO) δ 51.4, 54.9, 61.5, 111.1, 113.2, 121.3, 124.3, 126.5, 130.2, 130.4, 137.7, 138.1, 142.9, 144.3, 147.9, 150.2, 163.0, 165.9 ppm. Anal. calcd. for $C_{22}H_{18}BrN_5O_5$: C, 51.58; H, 3.54; N, 13.67. Found: C, 51.41; H, 3.67; N, 13.84.

*5-(4-{[1-(4-Bromobenzyl)-1*H*-1,2,3-triazol-5-yl]methoxy}-3-methoxybenzylidene)pyrimidine-2,4,6(1*H*,3*H*,5*H*)-trione (**8h**)*

White solid; yield: 78%, mp: 211–213°C. IR (KBr): 1,688 (C═O), 1,639 (C═C alkene), 2,922 (C–H aromatic) cm^{-1}. ^{1}H NMR (500 MHz, DMSO-d_6) δ 3.59 (s, 3H, OCH_3), 5.02 (s, 2H, N–CH_2), 5.59 (s, 2H, O–CH_2), 5.92 (s, 1H, alkene), 6.56 (s, 1H, Ar), 6.64 (s, 1H, Ar), 6.89 (d, J = 8.2 Hz, 1H, Ar), 7.28 (d, J = 8.1 Hz, 2H, Ar), 7.57 (d, J = 8.1 Hz, 2H, Ar), 8.25 (s, 1H, triazole), 10.10 (s, 2H, NH). ^{13}C NMR (126 MHz, DMSO) δ 51.4, 55.4, 61.7, 111.8, 113.4, 118.8, 121.4, 124.0, 129.7, 131.1, 134.9, 137.7, 142.9, 144.3, 147.9, 150.2, 163.3, 165.5 ppm. Anal. calcd. for $C_{22}H_{18}BrN_5O_5$: C, 51.58; H, 3.54; N, 13.67. Found: C, 51.33; H, 3.39; N, 13.51.

*5-(3-Methoxy-4-{[1-(4-nitrobenzyl)-1*H*-1,2,3-triazol-5-yl)methoxy}-benzylidene}pyrimidine-2,4,6(1*H*,3*H*,5*H*)-trione (**8i**)*

White solid; yield: 70%, mp: 201–207°C. IR (KBr): 1,336–1,352 (NO_2), 1,678 (C═O), 1,605 (C═C alkene), 3,035 (C–H aromatic) cm^{-1}. ^{1}H NMR (500 MHz, DMSO-d_6) δ 3.60 (s, 3H, OCH_3), 5.13 (s, 2H, N–CH_2), 5.99–5.72 (m, 3H), 7.09 (s, 1H, Ar), 7.45–7.29 (m, 1H, Ar), 7.56 (d, J = 8.2 Hz, 2H, Ar), 8.48–8.17 (m, 4H), 10.02–9.52 (m, 2H, NH). ^{13}C NMR (126 MHz, DMSO) δ 47.6, 51.1, 55.0, 61.6, 112.5, 113.0, 118.7, 123.4, 124.0, 125.4, 128.5, 130.8, 137.8, 138.5, 139.2, 143.4, 149.8, 150.3, 163.9, 165.3, 167.4 ppm. Anal. calcd. for $C_{22}H_{18}N_6O_7$: C, 55.23; H, 3.79; N, 17.57. Found; C, 55.37; H, 3.84; N, 17.65.

*5-(3-Methoxy-4-{[1-(2-methylbenzyl)-1*H*-1,2,3-triazol-5-yl]methoxy}-benzylidene)-2-thioxodihydropyrimidine-4,6(1*H*,5*H*)-dione (**8j**)*

White solid; yield: 86%, mp: 96–98°C. IR (KBr): 1,715 (C═O), 1,646 (C═C alkene), 2,928 (C–H aromatic) cm^{-1}. ^{1}H NMR (500 MHz, DMSO-d_6) δ 2.30 (CH_3, s, 3H), 3.59 (s, 3H, OCH_3), 5.03 (s, 2H, N–CH_2), 5.61 (s, 2H, O–CH_2), 5.93 (s, 1H, alkene), 6.89 (d, J = 8.4 Hz, 1H, Ar), 7.06 (s, 2H, Ar), 7.18 (s, 1H, Ar), 7.23 (s, 2H, Ar), 7.32 (s, 1H, Ar), 8.12 (s, 1H, triazole), 10.04 (s, 2H, NH) ppm. ^{13}C NMR (126 MHz, DMSO) δ 18.07, 43.92, 50.36, 54.95, 113.04, 118.28, 120.33, 122.44, 124.12, 125.70, 127.74, 128.07, 128.17, 129.85, 129.91, 129.95, 133.60, 133.71, 135.71, 142.62, 154.63, 161.75 ppm. Anal. calcd. for $C_{23}H_{21}N_5O_4S$: C, 59.60; H, 4.57; N, 15.11. Found: C, 59.74; H, 4.68; N, 15.01.

*5-(4-{[1-(2-Fluorobenzyl)-1*H*-1,2,3-triazol-5-yl]methoxy}-3-methoxybenzylidene)-2-thioxodihydropyrimidine-4,6(1*H*,5*H*)-dione (**8k**)*

White solid; yield: 87%; mp: 108–110°C. IR (KBr): 1,713 (C═O), 1,653 (C═C alkene), 2,919 (C–H aromatic) cm^{-1}. ^{1}H NMR (500 MHz,

DMSO-d_6) δ 3.71 (s, 3H, OCH_3), 5.11 (s, 2H, N–CH_2), 5.74–5.61 (m, 3H), 7.07 (s, 2H, Ar), 7.22 (t, J = 7.6 Hz, 1H, Ar), 7.27 (d, J = 9.5 Hz, 1H, Ar), 7.34–7.30 (m, 2H, Ar), 7.44–7.40 (m, 1H, Ar), 8.25 (s, 1H, triazole), 10.11 (m, 2H, NH) ppm. ^{13}C NMR (126 MHz, DMSO) δ 42.09, 46.03, 52.96, 109.02, 110.11, 111.14, 111.79, 116.31, 118.36, 122.29, 122.88, 126.46, 127.84, 129.08, 133.41, 136.23, 140.27, 142.54, 145.98, 149.26, 161.21, 170.28 ppm. Anal. calcd. for $C_{22}H_{18}FN_5O_4S$: C, 56.53; H, 3.88; N, 14.98. Found: C, 56.69; H, 3.74; N, 15.07.

*5-(4-{[1-(2-Chlorobenzyl)-1H-1,2,3-triazol-5-yl]methoxy}-3-methoxybenzylidene)-2-thioxodihydropyrimidine-4,6(1H,5H)-dione (**8l**)*

White solid; yield: 68%, mp > 250°C. IR (KBr): 1,703 (C=O), 1,643 (C=C alkene), 2,928 (C–H aromatic) cm^{-1}. ^{1}H NMR (500 MHz, DMSO-d_6) δ 3.61 (s, 3H, OCH_3), 5.05 (s, 2H, N–CH_2), 5.72 (s, 2H, O–CH_2), 5.92 (s, 1H, alkene), 6.57 (d, J = 8.3 Hz, 1H, Ar), 6.64 (s, 1H, Ar), 6.89 (d, J = 8.4 Hz, 1H, Ar), 7.18 (s, 1H, Ar), 7.43–7.30 (m, 2H, Ar), 7.52 (d, J = 7.8 Hz, 1H, Ar), 8.22 (s, 1H, triazole), 10.09 (s, 2H, NH). ^{13}C NMR (126 MHz, DMSO) δ 50.0, 54.9, 61.5, 111.1, 113.4, 118.8, 124.5, 127.2, 129.8, 132.0, 137.8, 142.7, 144.3, 148.0, 150.2, 163.3, 165.3 ppm. Anal. calcd. for $C_{22}H_{18}FN_5O_4S$: C, 54.60; H, 3.75; N, 14.47. Found: C, 54.72; H, 3.63; N, 14.58.

*5-(4-{[1-(4-Chlorobenzyl)-1H-1,2,3-triazol-5-yl]methoxy}-3-methoxybenzylidene)-2-thioxodihydropyrimidine-4,6(1H,5H)-dione (**8m**)*

White solid; yield: 76%, mp: 111–113°C. IR (KBr): 1,706 (C=O), 1,648 (C=C alkene), 2,926 (C–H aromatic) cm^{-1}. ^{1}H NMR (500 MHz, DMSO-d_6) δ 3.60 (s, 3H, OCH_3), 5.02 (s, 2H, N–CH_2), 5.61 (s, 2H, O–CH_2), 5.92 (s, 1H, alkene), 6.53 (d, J = 9.3 Hz, 1H, Ar), 6.91 (d, J = 9.1 Hz, 1H, Ar), 7.07 (d, J = 4.5 Hz, 1H, Ar), 7.35 (d, J = 8.0 Hz, 4H, Ar), 8.24 (s, 1H, triazole), 10.02 (s, 2H, NH) ppm. ^{13}C NMR (126 MHz, DMSO) δ 51.01, 55.89, 62.51, 112.13, 114.24, 119.29, 125.47, 128.19, 130.66, 130.83, 133.00, 133.74, 138.83, 143.71, 145.27, 148.97, 165.04, 167.20, 170.06 ppm. Anal. calcd. for $C_{22}H_{18}FN_5O_4S$: C, 54.60; H, 3.75; N, 14.47. Found C, 54.47; H, 3.76; N, 14.61.

*5-(4-{[1-(3-Bromobenzyl)-1H-1,2,3-triazol-5-yl]methoxy}-3-methoxybenzylidene)-2-thioxodihydropyrimidine-4,6(1H,5H)-dione (**8n**)*

White solid; yield: 73%, mp: 215–217°C. IR (KBr): 1,701 (C=O), 1,630 (C=C alkene), 2,924 (C–H aromatic) cm^{-1}. ^{1}H NMR (500 MHz, DMSO-d_6) δ 3.73 (s, 3H, OCH_3), 5.19 (s, 2H, N–CH_2), 5.65 (s, 2H, O–CH_2), 5.92 (s, 1H, alkene), 7.24 (s, 1H, Ar), 7.33 (s, 3H, Ar), 7.41 (s, 1H, Ar), 7.48 (s, 1H, Ar), 7.64 (s, 1H, Ar), 8.24 (s, 1H, triazole), 9.78 (s, 2H, NH). ^{13}C NMR (126 MHz, DMSO) δ 49.6, 54.9, 61.1, 109.2, 112.2, 125.0, 125.2, 127.4, 128.6, 129.4, 131.5, 133.5, 141.6, 146.2, 148.8, 152.2, 166.4, 168.7, 172.7 ppm. Anal. calcd. for $C_{22}H_{18}BrN_5O_4S$: C, 50.01; H, 3.43; N, 13.25. Found: C, 54.15; H, 3.55; N, 13.37.

4.2 | Biological evaluations

4.2.1 | Urease inhibitory assay

All chemicals and urease (JBU; EC 3.5.1.5) were purchased from Sigma-Aldrich. Urease inhibition assay of compounds **8a–n** was screened at the concentration of 0–10 mg/ml by the modified spectrophotometric method developed by Berthelot using alkaline phenol–hypochlorite reaction.[26] This method is based on the reaction of ammonia (NH_3) with hypochlorite (OCl^-) to form a monochloramine and a subsequent reaction of monochloramine with phenol to form blue-colored indophenols whose absorbance is measured at 625 nm.[16] The assay mixture solution consisted of urea (850 µl, 30 mM, in phosphate buffer 100 mM, pH 7.4) and test compounds (100 µl [0–10 mg/ml], phosphate buffer 100 mM, pH 7.4) with a total volume of 950 µl. The reactions were initiated by the addition of 15 µl of urease enzyme solution in phosphate buffer (100 mM, pH 7.4, 3 mg/ml). Urease activity was determined by measuring ammonia concentration after 30 min of enzymatic reaction. The ammonia concentration was determined by adding 100 µl incubated solution to a mixture of 500 µl of solution A (containing 5.0 g phenol and 25 mg of sodium nitroprusside in 500 ml distilled water) and 500 µl of solution B (contained 2.5 g sodium hydroxide and 4.2 ml of sodium hypochlorite [5% chlorine] in 500 ml distilled water) and again incubated at 37°C for 30 min. The absorbance of developed blue-colored indophenols was read at 625 nm. The activity of uninhibited urease was designated as the control activity of 100%. Hydroxyurea and thiourea were used as positive controls. The percentage of inhibition was determined according to this formula: $[1 - (T/C)] \times 100$, where T is the absorbance of the test compound in the presence of enzyme and C is the absorbance of the solvent as negative control in the presence of enzyme. The mean and standard error of the mean was calculated from data of three independent experiments and calculated by SPSS v16. IC_{50} values for all compounds **8a–n** were calculated using GraphPad Prism 5 software (GraphPad Software Inc., San Diego, CA).

4.2.2 | Kinetic study

To determine the type of urease inhibition of the synthesized compounds, Lineweaver–Burk plots were used according to literature.[27] Urease inhibition was measured by varying the concentrations of urea (1–4 mM) in the presence of different concentrations of the most potent compound **8l** (0, 5, 10, 15 µM). The inhibitory constant (K_i) was determined from secondary replotting of Lineweaver–Burk plots. All experiments were conducted in triplicate.

4.2.3 | Molecular modeling procedure

To find out the interaction mode of designed molecules over urease enzyme, Maestro Molecular Modeling platform (version10.5) by

Schrödinger LLC was employed.[28] The X-ray crystallographic structure of JBU (in complex with AHA) was downloaded from the Protein Data Bank (PDB ID: 4H9M; www.rcsb.org). As urease is reported to be functionally active in the monomeric state, all the docking studies were performed on a single monomer. In addition, prosthetic group and cofactors were not directly involved in urease inhibition, so they were totally removed before docking investigation. Water molecules and co-crystallized ligands were removed from the enzymes' crystallographic structures. The 2D structures of all synthesized compounds were drawn in Marvin 15.10.12.0 program (http://www.chemaxon.com) and converted into a pdb file. The Protein Preparation Wizard and the LigPrep module were used to prepare protein and ligand structure properly.[12] The missing side chains of the proteins were filled using the Prime tool and missing residues were updated.

The accurate side chain, backbone conformational changes, or both during ligand binding at the active site of urease enzyme were predicted by induced fit docking (IFD) method using Glide software (Schrödinger LLC, 2018). The AHA binding site was used to generate the grid for IFD calculation. The maximum 20 poses with receptor and ligand van der Waals radii of 0.7 and 0.5, respectively, were considered. Residues within 5 Å of the AHA at the active site were refined, followed by side chain optimization. Structures whose Prime energy was more than 30 kcal/mol were eliminated on the basis of extra precious Glide docking.

4.2.4 | Molecular dynamic simulation

Molecular simulations of this study were performed using the Desmond v5.3 using Maestro interface (from Schrödinger 2018-4 suite). The appropriate pose for MD simulation procedure of the compounds was achieved by the IFD method.

To build the system for MD simulation, the protein–ligand complexes were solvated with simple point-charge explicit water molecules and placed in the center of an orthorhombic box of appropriate size under the periodic boundary condition. Sufficient counter ions and a 0.15-M solution of NaCl were also utilized to neutralize the system and to simulate the real cellular ionic concentrations, respectively. The MD protocol involved minimization, pre-production, and finally production of MD simulation steps. In the minimization procedure, the entire system was allowed to relax for 2,500 steps by the steepest descent approach. Then the temperature of the system was increased from 0 to 300 K with a small force constant on the enzyme to restrict any drastic changes. MD simulations were performed via an NPT (constant number of atoms; constant pressure, i.e., 1.01325 bar; and constant temperature, i.e., 300 K) ensemble. The Nose–Hoover chain method was used as the default thermostat with 1.0-ps interval and Martyna–Tobias–Klein as the default barostat with 2.0-ps interval by applying isotropic coupling style. Long-range electrostatic forces were calculated on the basis of particle mesh-based Ewald approach with the cut-off radius for Columbic forces set at 9.0 Å. Finally, the system was subjected to produce MD simulations for 30 ns for each protein–ligand complex. During the simulation, every 1,000 ps of the actual frame was stored. The dynamic behavior and structural changes of the systems were analyzed by the calculation of the RMSD and RMSF. Subsequently, the energy-minimized structure calculated from the equilibrated trajectory system was evaluated for investigation of each ligand–protein complex interaction.

4.2.5 | Prediction of pharmacokinetic properties

The MW and log*P* values of the synthesized compounds **8a**–**n** were calculated using ChemDraw 18.2. HBD and HBA were calculated by the means of MarvineSketch 5.10.4. RBC was calculated using AutoDock Tools (ver. 1.5.6). Furthermore, ADMET prediction of the synthesized compounds was performed by preADMET online server (http://preadmet.bmdrc.org/).[29]

4.2.6 | Cytotoxicity

In vitro cytotoxicity was determined by the MTT assay in triplicate according to the literature.[30]

ORCID

Saghi Sepehri http://orcid.org/0000-0001-7340-0468
Mohammad Mahdavi http://orcid.org/0000-0002-4171-7310

REFERENCES

[1] S. Eidt, M. Stolte, R. Fischer, *J. Clin. Pathol.* **1994**, *47*, 436.
[2] M. R. Amieva, E. M. El-Omar, *Gastroenterology* **2008**, *134*, 306.
[3] H. Rautelin, K. Seppälä, O. V. Renkonen, U. Vainio, T. U. Kosunen, *Antimicrob. Agents Chemother.* **1992**, *36*, 163.
[4] H. Raza, Q. Abbas, M. Hassan, S. H. Eo, Z. Ashraf, D. Kim, A. R. Phull, S. J. Kim, S. K. Kang, S. Y. Seo, *Pharm. Biol.* **2017**, *55*, 218.
[5] M. S. Refat, A. M. Adam, *J. Mol. Liq.* **2014**, *196*, 142.
[6] M. T. Omar, *Egypt. J. Pharm. Sci.* **1997**, *38*, 281.
[7] M. Kidwai, R. Thakur, R. Mohan, *Acta Chim. Slov.* **2005**, *52*, 88.
[8] A. Barakat, M. S. Islam, A. M. Al-Majid, H. A. Ghabbour, S. Yousuf, M. Ashraf, N. N. Shaikh, M. I. Choudhary, R. Khalil, Z. Ul-Haq, *Bioorg. Chem.* **2016**, *68*, 72.
[9] J. A. Vida, W. R. Wilber, J. F. Reinhard, *J. Med. Chem.* **1971**, *14*, 190.
[10] A. Rauf, F. Ahmed, A. M. Qureshi, A. Khan, M. I. Qadir, M. I. Choudhary, Z. H. Chohan, M. H. Youssoufid, T. B. Haddad, *J. Chin. Chem. Soc.* **2011**, *58*, 528.
[11] A. Lauria, R. Delisi, F. Mingoia, A. Terenzi, A. Martorana, G. Barone, A. M. Almerico, *J. Med. Chem.* **2014**, 3289.
[12] H. Azizian, F. Nabati, A. Sharifi, F. Siavoshi, M. Mahdavi, M. Amanlou, *J. Mol. Model.* **2012**, *18*, 2917.
[13] F. Rahim, M. Ali, S. Ullah, U. Rashid, H. Ullah, M. Taha, M. T. Javed, W. Rehman, A. A. Khan, O. U. Abid, M. Bilal, *Chin. Chem. Lett.* **2016**, *27*, 693.
[14] M. Vosooghi, S. Farzipour, M. Saeedi, N. B. Shareh, M. Mahdavi, S. Mahernia, A. Foroumadi, M. Amanlou, A. Shafiee, *J. Iran. Chem. Soc.* **2015**, *12*, 1487.
[15] M. Asadi, M. Mahdavi, S. Mahernia, Z. Rezaei, M. Safavi, M. Saeedi, M. Amanlou, *Lett. Drug Des. Discov.* **2018**, *15*, 428.
[16] S. Moghimi, F. Goli-Garmroodi, M. Allahyari-Devin, H. Pilali, M. Hassanzadeh, S. Mahernia, M. Mahdavi, L. Firoozpour, M. Amanlou, A. Foroumadi, *Arch. Pharm.* **2018**, *351*, e1800005.

[17] A. Barakat, S. M. Soliman, M. Ali, A. Elmarghany, A. M. Al-Majid, S. Yousuf, Z. Ul-Haq, M. I. Choudhary, A. El-Faham, *Inorg. Chim. Acta* **2020**, *503*, 119405.
[18] M. Alomari, M. Taha, S. Imran, W. Jamil, M. Selvaraj, N. Uddin, F. Rahim, *Bioorg. Chem.* **2019**, *92*, 103235.
[19] M. A. Abbasi, M. Hassan, S. Z. Siddiqui, H. Raza, S. A. A. Shah, S. Y. Seo, *Bioorg. Med. Chem.* **2018**, *26*, 3791.
[20] N. C. Ha, S. T. Oh, J. Y. Sung, K. A. Cha, M. H. Lee, B. H. Oh, *Nat. Struct. Mol. Biol.* **2001**, *8*, 505.
[21] X. Arqué, A. Romero-Rivera, F. Feixas, T. Patiño, S. Osuna, S. Sánchez, *Nat. Commun.* **2019**, *10*, 1.
[22] C. A. Lipinski, *J. Pharmacol. Toxicol. Methods* **2000**, *44*, 235.
[23] D. F. Veber, S. R. Johnson, H. Y. Cheng, B. R. Smith, K. W. Ward, K. D. Kopple, *J. Med. Chem.* **2002**, *45*, 2615.
[24] Z. Bakherad, M. Mohammadi-Khanaposhtani, H. Sadeghi-Aliabadi, S. Rezaei, A. Fassihi, M. Bakherad, H. Rastegar, M. Biglar, L. Saghaie, B. Larijani, M. Mahdavi, *J. Mol. Struct.* **2019**, *1192*, 192.
[25] M. S. Asgari, M. Mohammadi-Khanaposhtani, M. Kiani, P. R. Ranjbar, E. Zabihi, R. Pourbagher, R. Rahimi, M. A. Faramarzi, M. Biglar, B. Larijani, M. Mahdavi, *Bioorg. Chem.* **2019**, *92*, 103206.
[26] F. Nabati, M. Habibi-Rezaei, M. Amanlou, A. A. Moosavi-Movahedi, *J. Mol. Catal. B: Enzym.* **2011**, *70*, 17.
[27] L. Tan, C. Li, H. Chen, Z. Mo, J. Zhou, Y. Liu, Z. Ma, Y. Xu, X. Yang, J. Xie, Z. Su, *Eur. J. Pharm. Sci.* **2017**, *110*, 77.
[28] L. L. Schrodinger, *Schrodinger Suite 2012 Induced Fit Docking protocol; Glide version 5.8*, Schrodinger, LLC, 2012, New York, NY.
[29] PreADMET, Seoul, South Korea, Bioinformatics and Molecular Design Research Center; 2020. PreADMET program, http://preadmet.bmdrc.org
[30] M. H. Abolhasani, M. Safavi, M. T. Goodarzi, S. M. Kassaee, M. Azin, *DARU J. Pharm. Sci.* **2018**, *26*, 105

SUPPORTING INFORMATION

Additional supporting information may be found online in the Supporting Information section.

How to cite this article: Asgari MS, Azizian H, Nazari Montazer M, et al. New 1,2,3-triazole–(thio)barbituric acid hybrids as urease inhibitors: Design, synthesis, in vitro urease inhibition, docking study, and molecular dynamic simulation. *Arch Pharm*. 2020;e2000023.
https://doi.org/10.1002/ardp.202000023